

Unravelling Malaria Antigen Binding to Antibody-Gold Nanoparticle Conjugates

Miguel A. S. Cavadas, Marco P. Monopoli, Cláudia Sá e Cunha, Miguel Prudêncio, Eulália Pereira, Iseult Lynch, Kenneth A. Dawson, and Ricardo Franco*

Conjugates formed by antibody adsorption to gold nanoparticles (AuNP) have found extensive utilization in immunoassays due to the high surface area and interesting optical and electronic properties of the nanomaterials. Nevertheless, the mechanism of formation of antibody-AuNP conjugates and their antigen binding characteristics have not been sufficiently explored in terms of specificity and consequent clinical applicability. Dynamic light scattering and related techniques have been successfully employed to detect antigen binding to antibody-AuNP complexes. Here, a range of different techniques from the bionanotechnology realm have been applied to obtain a detailed picture of a competitive immunoassay for malaria antigen detection, based on fluorescence-quenching by AuNPs. Both agarose gel electrophoresis and differential centrifugal sedimentation (DCS) analyses provide binding constants in the same order of magnitude, for antibody binding to AuNP and for antigen binding to antibody-AuNP conjugates. Both techniques are also able to reveal inhibition of antigen binding in the presence of a major blood plasma protein, transferrin (via competitive binding). DCS is further used to show inhibition of the binding of the antigen in the presence of human plasma, a realistic testing condition, of high relevance to the implementation of immunoassays at the clinical level.

1. Introduction

Biomarker discovery and analysis are of fundamental importance for health improvement.^[1] In infectious diseases such as malaria, early diagnosis is of critical importance for efficient patient treatment and increased survival rates.^[2] The biggest barrier to biomarker discovery is their extremely low concentration in biological fluids such as plasma, which contains over 3700 different proteins with concentrations ranging from $\approx 50 \text{ mg mL}^{-1}$ (albumin) to a few pg/mL of most other plasma proteins.^[3] Nanotechnology can provide improved detection of low abundance biomarkers by biomarker harvesting via specific affinity for the nanoparticle surface and/or concentration at the nanoparticle surface.^[4] Optimization of existing technologies (e.g., ELISA, chemiluminescence or electrochemical methodologies) and development of new diagnostics platforms, such as bio-barcode

Dr. M. A. S. Cavadas,^[†] R. Franco

UCIBIO

REQUIMTE

Departamento de Química
Faculdade de Ciências e Tecnologia
Universidade NOVA de Lisboa
2829-516 Caparica, Portugal
E-mail: ricardo.franco@fct.unl.pt

Dr. M. A. S. Cavadas, Prof. K. A. Dawson
Centre for BioNano Interactions and Conway Institute for Biomolecular and Biomedical Research
School of Chemistry & Chemical Biology
University College Dublin
Belfield, Dublin 4, Ireland

Dr. M. A. S. Cavadas
Systems Biology Ireland
Conway Institute for Biomolecular and Biomedical Research
University College Dublin
Belfield, Dublin 4, Ireland

Dr. M. P. Monopoli
RCSI Pharmaceutical and Medical Chemistry
Royal College of Surgeons in Ireland
Dublin 2, Ireland

DOI: 10.1002/ppsc.201600187

Dr. C. Sá e Cunha, Dr. M. Prudêncio
Instituto de Medicina Molecular
Faculdade de Medicina da Universidade de Lisboa
1649-028, Lisboa, Portugal

Prof. E. Pereira
UCIBIO
REQUIMTE
Departamento de Química e Bioquímica
Faculdade de Ciências
Universidade do Porto
4169-007, Porto, Portugal

Prof. I. Lynch
School of Geography
Earth & Environmental Sciences
University of Birmingham
Edgbaston, B17 0JN, Birmingham, UK

^[†]Present address: Instituto Gulbenkian de Ciência, R. Qta Grande 6, 2780-156 Oeiras, Portugal



assays, and gold- and magnetic-nanoparticle-based fluorescence quenching assays,^[5] is also envisaged. Gold nanoparticles are especially promising by virtue of their signal-enhancing capabilities.^[5,6] While some strategies that take advantage of the special properties of gold nanoparticles (AuNPs), e.g., the hydrogel nanoparticle-based strategy, are still in early, proof-of-principle stages, the use of AuNPs for the specific detection of nucleic acid sequences and immunoassays on lateral flow formats are currently being used for the analysis of clinical samples.^[6b,7] Huo and co-workers developed a label-free assay based on gold nanoparticle-antibody conjugates, to detect prostate specific antigen (PSA).^[8] The method is based on two distinct types of gold nanoparticles, spherical and rod-shaped, each functionalized with a different antibody, for capture and detection, respectively. PSA antigen in simulated human serum samples induces the formation of self-assembled nanoparticle oligomers and aggregates that can be detected by dynamic light scattering (DLS). This single-step, wash-free, homogeneous immunoassay has been of great interest and value to the scientific community, being the AuNP-based immunoassay with the highest number of citations in the literature. In fact, simple, label-free methods that combine the specificity and sensitivity of antibody-antigen detection with ease of operation, even in low-resource settings, are the method of choice for biomarker detection and have the highest potential for translation into clinical settings. Nevertheless, the characterization of AuNP-Ab conjugate formation and the mode of antigen binding to the conjugate have been elusive to date. Such detailed characterization is hampered by a lack of methodologies for analysis of bioconjugate/ligand complexes, especially under competitive binding conditions. The orientation of antibodies on AuNP-Ab conjugates has revealed improved antigen-binding efficacies. Nevertheless, these studies relied on additional conjugation steps of protein A/G intermediates,^[9] or EDC chemistry at a PEGylated-AuNP surface.^[10] Recent studies have revealed differential adsorption of proteins to NPs in complex samples (e.g., human plasma) with lower abundance proteins with higher affinity for NP surfaces quickly replacing lower affinity, higher abundance proteins.^[11] The highest affinity proteins have been shown to adhere to NPs for several hours, even under conditions where chemical potentials would suggest that the proteins should dissociate from the NP surface.^[11c,12] Studies have shown that the protein layer covering the NPs, also called the “protein corona”, is composed of an inner layer of selected proteins with a lifetime of several hours in slow exchange with the environment (hard corona),^[12,13] and an outer layer of weakly bound proteins which are characterized by a faster exchange rate with the free proteins (the soft corona).^[12–14]

In this work, we investigated the specificity of binding of 30 nm citrate-capped AuNPs conjugated with a mouse IgG monoclonal antibody (2E6) that specifically recognizes *Plasmodium falciparum* (Pf) heat shock protein 70 (PfHsp70), an antigen used in malaria diagnostics, expressed in infected erythrocytes and detectable in infected patients.^[15] The 2015 World Malaria Report, which summarizes information received from 96 malaria-endemic countries, estimated that 3.2 billion people are at risk of being infected by *Plasmodium* and developing malaria. In 2015, there were an estimated 214 million cases of malaria, which resulted in 438 000 deaths, 90% of which in sub-Saharan

Africa.^[2] Such figures imply an urgent need for well-designed, reliable, and inexpensive diagnostic assays. Thus, there is significant interest in the assessment of new methodologies to evaluate the binding efficiency of bioconjugated NPs in order to design assays with better functionality and reliability for early detection of infection.

Our goal is to assess easily available techniques to characterize the density of Ab adsorbed around the AuNPs and thus determine its structure in terms of monolayer or multilayer structure, the agglomeration state of the AuNP-Ab conjugates, and the influence of these factors on the availability of antigen binding sites. Furthermore, we provide a comprehensive description of antigen (Hsp70) binding to the AuNP-Ab conjugates, at an extensive range of Hsp70-to-Ab concentration ratios. In addition, antigen-binding constants to AuNP-Ab conjugates were determined for the first time. Finally, examples of competitive interference from transferrin, one of the most abundant plasma proteins, and from whole plasma, are presented, indicating how the assay can function even under realistic biological conditions. Complex mixtures, such as plasma, are often encountered when AuNP-Ab conjugates are used in immunoassays of blood-derived samples, clearly highlighting the need to test detection systems under the actual usage conditions, before drawing conclusions regarding their efficacy.

We have used three different but complementary techniques, namely, differential centrifugal sedimentation (DCS); agarose gel electrophoresis (AGE); and fluorescence spectroscopy, to study the AuNP-Ab-Hsp70 interactions. The fluorimetric determinations constitute the basis of a homogenous competitive immunoassay, and correspond to fluorescence quenching of a dye-labeled antigen when bound to a AuNP-Ab conjugate. In the absence of analyte antigen, the labeled antigen remains bound to the AuNP-Ab conjugate and the fluorescence is quenched. In the presence of analyte antigen, the labeled antigen is competitively released from the AuNP-Ab conjugate binding sites, leading to a fluorescence increase.^[15] These findings were confirmed by the DCS and AGE experimental approaches.

2. Results and Discussion

Our model system was an antibody-antigen system employed in malaria diagnosis. Thus, throughout this work, “Ab” refers to the mouse IgG monoclonal antibody (2E6) that specifically recognizes the antigen, *Plasmodium falciparum* heat shock protein 70 (PfHsp70), simply referred to as “Hsp70”.

2.1. Gold Nanoparticle-Antibody Conjugates (AuNP-Ab)

Gold nanoparticle-antibody conjugates (AuNP-Ab) were prepared by simple incubation in buffer using Ab:AuNP molar ratios in the range 5:1 to 1000:1 (see the Experimental Section). The resulting conjugates were characterized by UV-vis spectroscopy, DLS, DCS, and AGE. Ab to AuNP conjugation was evident from UV-vis spectra, with a 6 nm red shift of the surface plasmon resonance of the AuNPs (Figure 1). DLS measurements confirmed that the AuNP-Ab complexes were stable in solution and further indicated a ≈ 10 nm increase of the

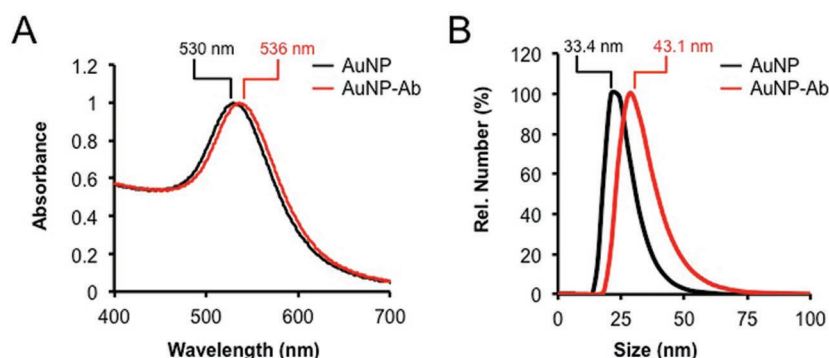


Figure 1. UV/vis and DLS characterization of Ab conjugation to AuNPs. A) UV-vis spectra of AuNP (black trace) and AuNP-Ab conjugates (red trace). A 6 nm red shift is observed upon Ab conjugation. Ab to AuNP molar ratio is 200:1 and AuNP concentration is 0.28×10^{-9} M. Spectra were normalized to the LSPR maximum; B) AuNP size increase upon Ab conjugation determined by DLS. AuNPs (black trace) exhibit a size increase upon antibody conjugation, AuNP-Ab (red trace). Each distribution averages three independent experiments, each with three measurements of 20 acquisition cycles. Ab to AuNP molar ratio is 200:1 and AuNP concentration is 0.058×10^{-9} M.

hydrodynamic radius compared to AuNPs alone (Figure 1) confirming binding of the Ab. An increase of the colloidal stability of AuNP-Ab conjugates compared to AuNPs alone in 75×10^{-3} M NaCl was observed, as evaluated by salt-induced agglomeration of AuNP-Ab conjugates (Figure S1A, Supporting Information). Salt-induced agglomeration is caused by cancelling of the charge-screening effect of the citrate-capping present in AuNPs, and so the presence of the Ab layer around the AuNPs has the observed effect of increasing AuNP colloidal stability.

Electrostatic adsorption of antibodies to the surface of AuNP is a very simple and extensively used method for conjugation.^[5] A well-known limitation of this procedure is the release of Ab upon changing the ionic strength and pH of the medium. Thus, we have used DCS (Figure S1B, Supporting Information) and UV-vis spectroscopy (Figure S1C, Supporting Information), to confirm the stability of the AuNP-antibody complexes in 75×10^{-3} M NaCl and at pH > 6, respectively. Taken together, these results show that the Ab remains conjugated to the AuNP surface at high ionic strength and at physiologically relevant pH values. Plasma osmolarity is about 300 mOsm, about 90% of which comes from NaCl.^[16] Knowing that these conjugates are stable at 75×10^{-3} M NaCl, a maximum of 50% (V/V) plasma could be used in point-of-care immunoassays.

DCS measurements of AuNPs alone and with increasing Ab:AuNP molar ratios indicate that both AuNPs and AuNP-Ab conjugates are stable toward agglomeration in solution, with no detectable peaks for larger particles. AuNP-Ab conjugates were detected at a smaller apparent size compared to the citrate-capped AuNPs alone (Figure 2A), due to the formation of a lower-density Ab corona around the much denser AuNPs. The apparent size decreased with increasing antibody concentration, until a plateau was reached at an Ab:AuNP molar ratio of 200 Ab per AuNP. In order to obtain the effective size of the AuNP-Ab conjugates and the appropriate thickness of the Ab (i.e., protein) layer (nm) (Figure 2B), a simple core-shell two-density model was used. This model applies a correction for the change in density resulting from protein adsorption onto the core material for

the calculation of the volume of the proteins adsorbed (for details of the core-shell model see Supporting Information in Walczyk et al.^[13b]). The shell thickness of the Ab (protein) layer and its apparent diameter (D_{app}) was determined as a function of $[Ab]/[AuNP]$ ratios (Figure 2C). The calculated volume was then used to estimate the number of Ab molecules adsorbed per AuNP, assuming an Ab (protein) density of 1.125 g cm^{-3} and an Ab molecular weight of 150 kDa. The amount of AuNP-bound Ab can be fitted to a Langmuir isotherm (Equation (1), see the Experimental Section), with a binding constant on the order of 10^8 M^{-1} (Figure 2D). This value compares well with an affinity constant of 10^7 M^{-1} , which was previously obtained by zeta-potential measurements for AuNP-Ab conjugates with the same Ab and smaller diameter AuNPs (15 nm) with 11-mercaptoundecanoic acid as a capping agent.^[15]

AGE is an inexpensive electrophoresis technique, widely employed in the molecular biology field. It is mainly used to isolate large charged biomolecules, such as DNA and synthetic polymers. Since its inception by the Alivisato's group for the detailed and elegant structural elucidation of DNA strands attached to AuNPs,^[17] AGE has found vast application in the field of nanoparticle analysis, where NPs and bionanoconjugates are separated according to differences in size and surface charge.^[9,13a,18] Analysis of AuNP-Ab conjugates with increasing Ab:AuNP molar ratios by AGE (Figure 2E) confirmed the formation of a persistent Ab corona around the AuNPs. The calculated electrophoretic mobility ranges from $-1.5 \text{ } \mu\text{m cm V}^{-1} \text{ s}^{-1}$ (AuNPs alone) up to $-1.0 \text{ } \mu\text{m cm V}^{-1} \text{ s}^{-1}$ at Ab:AuNP molar ratios of $\approx 200:1$ and higher. This variation of electrophoretic mobility is consistent with a decrease of the negative charge due to Ab coverage of the AuNPs, and a simultaneous increase of the hydrodynamic volume of the AuNP-Ab-Hsp70 complex; both effects contribute to shorter migration lengths in the agarose gel. Also, the bands for lower Ab to AuNP molar ratios present noticeable smearing, becoming sharper for higher $[Ab]/[AuNP]$. This behavior seems to indicate that the formation of a hard Ab corona around the AuNP only occurs for $[Ab]/[AuNP]$ ratios above 200, in accordance with DCS observations. Thus, an Ab:AuNP ratio of 200:1 was used for the following experiments. AGE analysis also enables determination of the Ab-to-AuNP binding constant by fitting the electrophoretic mobility data to a Langmuir-type adsorption curve. The calculated affinity constant is in the order of 10^8 M^{-1} (Figure 2F), similar to that obtained by DCS.

2.2. Antigen Binding to AuNP-Ab Conjugates

Hsp70 antigen binding to AuNP-Ab conjugates, can be detected by a competitive immunoassay based on fluorescence recovery after quenching of fluorophore-labeled recombinant Hsp70 (Figure S2, Supporting Information).^[15] We employed AGE to assess Hsp70 binding to AuNP-Ab conjugates. To our

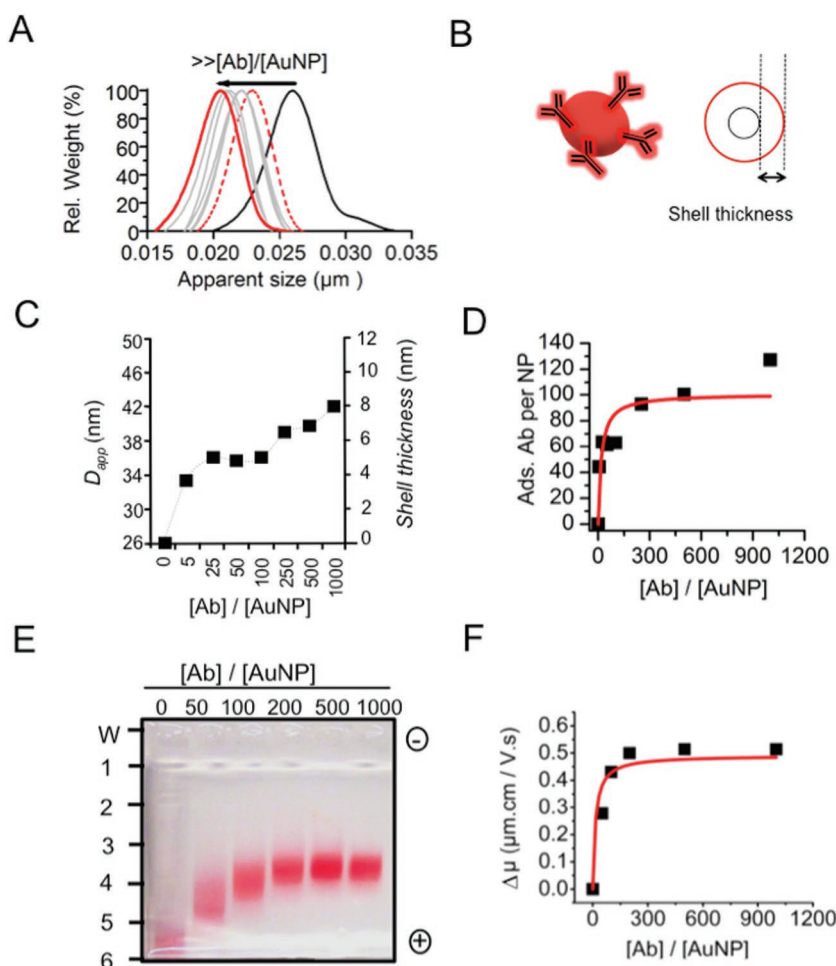


Figure 2. Characterization of AuNP-Ab by A–D) DCS, and E,F) AGE. (A) DCS profiles. The black trace corresponds to AuNPs alone. $[Ab]/[AuNP]$ varied between 5 (dashed red trace) and 1000 (full red trace). (B) A previously described core–shell model was used to calculate shell thickness (nm) and apparent diameter (D_{app}). See the Experimental Section for details. (C) Shell thickness and D_{app} as a function of $[Ab]/[AuNP]$ ratios, from 0 to 1000. (D) Langmuir-fitting data for the variation of the number of Ab adsorbed to AuNP, as determined by DCS, versus Ab:AuNP molar ratios. (E) 0.5% agarose gel of AuNP-Ab conjugates formed by incubation at the indicated Ab:AuNP molar ratios. The red color of the AuNPs is clearly visible on the agarose gels, and thus no staining was necessary. (F) Apparent relative electrophoretic mobility, fitted to a Langmuir-type curve.

knowledge, this is the first time that the electrophoretic gel shifts observed upon Hsp70 binding to AuNP-Ab conjugates have been used to characterize the antigen-to-Ab binding process.

Figure 3A shows a typical gel obtained with increasing AuNP-Ab:Hsp70 molar ratios. The electrophoretic mobility for the red band corresponding to AuNP-Ab-Hsp70 complexes, shifts linearly with Hsp70 concentration in the range of ≈ 1.5 –24 AuNP-Ab-Hsp70 molar ratios. This molar ratio range corresponds to an Hsp70 concentration in the range of 7.1 – $57 \mu\text{g mL}^{-1}$ ($R^2 = 0.977$ – Figure 3B), which agrees well with the linear response region observed for the fluorimetric immunoassay (Figure S2, Supporting Information). Such coherence of results defines a useful range for detecting low parasitemia levels in malaria-infected blood samples,^[15] raising the possibility of using this simple AGE method as a rapid clinical assay for Hsp70 detection.

DCS was employed to further characterize Hsp70 binding to AuNP-Ab conjugates via an independent and well-established bionanotechnology methodology. **Figure 4** presents DCS profiles for AuNP-Ab alone and incubated with Hsp70 for increasing AuNP-Ab-Hsp70 molar ratios (Figure 4B); or for increasing incubation time (Figure 4C). The AuNP-Ab-Hsp70 molar ratios assessed were in the range 3–120:1 for an incubation period of 120 min. Incubation time was varied from 1 to 420 min at an AuNP-Ab-Hsp70 molar ratio of 30:1.

Increasing the AuNP-Ab-Hsp70 molar ratios, changes the DCS profile from a single band to a signal containing at least two components. This behavior was fitted to a model of two Gaussian components, one centered at $0.021 \mu\text{m}$, corresponding to the AuNP-Ab conjugates alone, and the other centered at $0.014 \mu\text{m}$, corresponding to AuNP-Ab conjugates fully loaded with Hsp70 (Figure 4A). Note that the size of the fully Hsp70-loaded complex is apparently smaller than the unloaded complex (Figure 4A), but this is a consequence of the lower density of the Hsp70 compared to that of the AuNPs, as has been previously observed,^[13b] and also occurs in the case of Ab-loaded AuNPs (Figure 2A).

Using the values obtained from the simulations, we calculated the amount of fully loaded conjugates relative to the total amount of AuNP-Ab conjugates for the various Hsp70:AuNP molar ratios studied, and the results are presented in Figure 4B. Data for the formation of the AuNP-Ab-Hsp70 complex with increasing Hsp70 concentration were fitted to a binding isotherm (Equation (1), see the Experimental Section) with an affinity constant on the order of 10^6 M^{-1} , which is within the canonical range of antigen binding affinities for antibodies produced during an immune response, 10^5

to 10^9 M^{-1} .^[19] This corresponds to $\approx 80\%$ of the AuNP-Ab conjugates yielding AuNP-Ab-Hsp70 complexes at an AuNP-Ab-Hsp70 molar ratio of 120:1 and a fixed incubation time of 120 min. For higher AuNP-Ab-Hsp70 molar ratios, the AuNP-Ab conjugates conversion yields remain constant at $\approx 80\%$ (data not shown).

In a time-dependence study (Figure 4C), the changes in the DCS profile are similar, with signals containing at least two components being detected for an incubation period of 15 min or longer. In this case, also, the maximum corresponding to the Hsp70:AuNP-Ab conjugates shifts toward lower apparent sizes, indicating that the number of Hsp70 bound per AuNP-Ab increases with time. In accordance with the previous data, maximum load in this time range is attained at an apparent size of $0.014 \mu\text{m}$. After fitting the two-Gaussian components, we calculated the amount of fully loaded conjugates relative to the

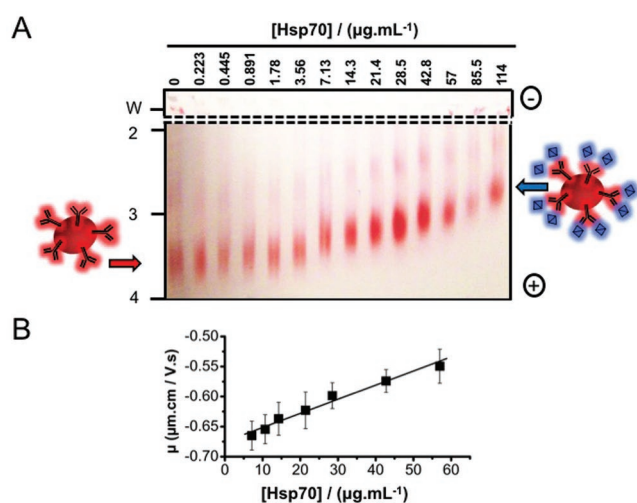


Figure 3. AGE of AuNP-Ab-Hsp70 complexes shows band shifting that is directly proportional to the concentration of bound Hsp70. A) 0.5% agarose gel of AuNP-Ab-Hsp70 complexes formed at the indicated Hsp70 concentrations. “W” marks the loading wells, vertical numbers indicate the migration distance in cm, “-” and “+” signs indicate the position of the electrodes. B) Calculated apparent electrophoretic mobility of AuNP-Ab-Hsp70 bands versus Hsp70 concentration. Data and error bars are from three independent experiments. Linear correlation coefficient: 97.7% (see the Experimental Section for details).

total amount of AuNP-Ab conjugates for the various AuNP-Ab-Hsp70 molar ratios studied, and the results are shown in the graph on the right of Figure 4C. In this case, 65% of the AuNP-Ab conjugates convert to AuNP-Ab-Hsp70 after a 420 min incubation period in the presence of a molar ratio of 30 Hsp70 per AuNP-Ab conjugate.

The two approaches (DCS and AGE) used for analysis of Hsp70 binding to the AuNP-Ab conjugate seem to reveal different Hsp70-to-Ab binding models. Two populations were detected by DCS corresponding to either fully Hsp70-charged AuNP-Ab or to AuNP-Ab with no Hsp70 bound, whereas by AGE only one population was detected, corresponding to partially Hsp70-charged AuNP-Ab complexes. This mode of Hsp70 binding to the AuNP-Ab conjugates as revealed by AGE experiments, is similar to the behavior observed for Ab to AuNP binding by both DCS and AGE, in which an Ab corona grows around the AuNP as the Ab concentration is increased. Conversely, the “all or nothing” behavior revealed by DCS for the mode of Hsp70 binding to the AuNP-Ab conjugates is certainly puzzling and a number of explanations might be put forth. First, it should be noted that the two techniques (AGE and DCS) were used under different experimental conditions. DCS experiments were performed at a $\approx 5\times$ higher Hsp70 concentration than AGE. In fact, the calculated limits of detection for both techniques were $20 \mu\text{g Hsp70 mL}^{-1}$ for DCS, and as low as $3.6 \mu\text{g Hsp70 mL}^{-1}$ for AGE. Second, although both techniques apply shear forces to the samples, the nature of those

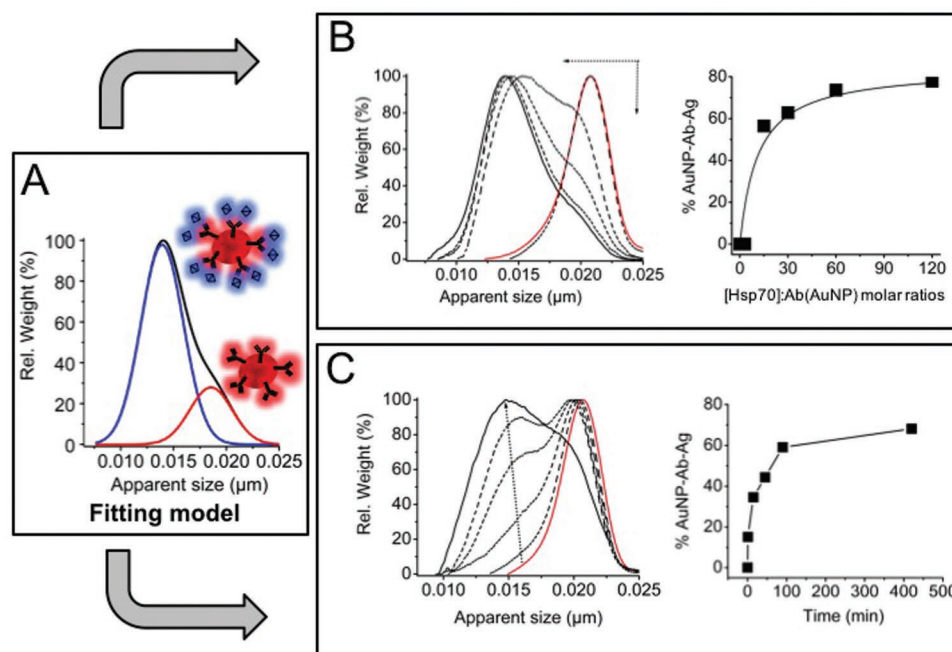


Figure 4. Variation of DCS profiles for AuNP-Ab-Hsp70 complexes with Hsp70 concentration and incubation time. A) The black line, corresponding to the experimental data, can be fitted by two components: (i) AuNP-Ab-Hsp70 complexes (blue line); and (ii) AuNP-Ab conjugates (red line). Schematics of the two complexes are also shown. B) DCS profiles for increasing Hsp70: AuNP-Ab molar ratios of 3, 15, 30, 60, and 120, for an incubation period of 120 min (black lines). The DCS profile for the AuNP-Ab conjugate alone ($93 \times 10^{-12} \text{ m}$; with a ratio of 70 Ab molecules adsorbed per AuNP, as determined by DCS) is shown in red. The relative amounts of AuNP-Ab-Hsp70 obtained by fitting the DCS profiles (graph on the right) were fitted to a binding isotherm. C) DCS profiles for increasing incubation times of 1, 15, 30, 45, 90, and 420 min, at an Hsp70:AuNP-Ab ratio of 30. The relative amounts of AuNP-Ab-Hsp70 obtained by fitting the DCS profiles are shown in the plot on the right (the line is a guide to the eye).

forces is intrinsically different, i.e., an electrical field in the case of AGE and mechanical centrifugation forces in the case of DCS. It can be speculated that shear forces are larger for DCS, favoring Hsp70 unbinding and leading to two independent species: AuNP-Ab conjugates and fully loaded AuNP-Ab-Hsp70 complexes. In AGE, the electrical field forces may not be strong enough to remove Hsp70 from the AuNP-Ab-Hsp70 complexes causing Hsp70 to appear uniformly distributed amongst all AuNP-Ab conjugates. A third possible explanation is that in AGE, only the antibody “hard corona” is observed, allowing a facilitated access of Hsp70 to the Ab binding sites and consequently a progressive binding of Hsp70 as its concentration increases. Conversely, in DCS experiments, a multitude of Ab and Hsp70 layers might be present as an intricate Ab/Hsp70 multilayer, exhibiting the observed cooperative behavior.

2.3. pH and Binding Forces

At the working pH values of 7.2–7.4, all of the biological molecules used are probably, globally negatively charged. In fact: (i) the isoelectric point for murine monoclonal antibodies, such as the one utilized, has been experimentally determined to be on the pH range 5.4–7.2;^[20] (ii) the theoretical isoelectric point for the antigen (*Pf*Hsp70) is 5.50, as determined by the “Compute pI/Mw” tool of ExpASy,^[21] for the nonrecombinant protein (lacking the 6XHis at its N-terminus); and (iii) for human transferrin, the described isoelectric point is 6.3–6.4.^[22] Interactions between AuNP-antibody; antibody-Hsp70; and between transferrin and the conjugates, are thus probably not electrostatically driven. The global negative charge of all the species involved at the working pH of 7.2–7.4 does not automatically imply that there are no local positively charged areas within the antibody/Hsp70/transferrin molecules, so there can be some electrostatic binding involved nevertheless. An important binding force between AuNPs and the antibody is the covalent binding between the antibody disulfide bridges and the AuNP surface,^[23] at least for the first antibody corona layer.

2.4. Competitive Binding

Assessing the interference of an individual plasma protein and of whole plasma on Hsp70 binding to the AuNP-Ab conjugates is of high relevance in the context of using AuNP-Ab conjugates for Hsp70 detection in *Plasmodium*-infected blood samples. In fact, non- or less specific binding of other proteins to the NP surface can interfere with the specificity and detection capabilities of the AuNP-Ab complexes.^[24] Therefore, we investigated the influence of both a single competitive binding plasma-protein, and of whole plasma, on Hsp70 binding to the Ab-AuNP conjugates.

2.4.1. Single Plasma-Protein Competitive Binding

The specificity of Hsp70 binding to the AuNP-Ab complexes was evaluated in the presence of transferrin (Trf), one of most abundant proteins in blood plasma,^[25] in order to assess the

binding ability of the Ab-AuNPs conjugates under competitive binding conditions.^[24] Control experiments using DCS and AGE to evaluate Trf binding to AuNP-Ab conjugates showed the absence of nonspecific interactions. In fact, no alterations were observed in either the DCS profiles or in migration shifts in AGE, for AuNP-Ab conjugates incubated with Trf (Figure S3, Supporting Information). Also, the fluorimetric immunoassay in the presence of Trf only (no Hsp70 analyte) did not show any significant fluorescence enhancement (data not shown). Taken together, these results indicate that AuNP-Ab conjugates exclude completely the binding of Trf, most probably due to the absence of interaction with the antibody.

Figure 5 shows DCS, AGE and fluorescence enhancement results for AuNP-Ab conjugates incubated in the presence of equimolar amounts of Hsp70 and Trf. The DCS profile is slightly affected by the presence of Trf, showing an increase in the proportion of the AuNP-Ab conjugate population relative to the AuNP-Ab-Hsp70 complex. In fact, using a two Gaussian curve model, the relative amount of AuNP-Ab-Hsp70 complex in the absence of Trf is 63%, whereas it decreases to 59% in the presence of Trf (Figure 5A).

Trf interference with Hsp70 binding to AuNP-Ab complexes was also confirmed by AGE. AGE analyses of AuNP-Ab conjugates incubated in the presence of Hsp70 and Trf shows a band with an intermediate electrophoretic mobility ($\mu = -0.68 \mu\text{m cm V}^{-1} \text{s}^{-1}$) between that of the AuNP-Ab conjugates alone ($\mu = -0.73 \mu\text{m cm V}^{-1} \text{s}^{-1}$), and AuNP-Ab-Hsp70 complexes ($\mu = -0.60 \mu\text{m cm V}^{-1} \text{s}^{-1}$) (Figure 5B).

As was observed in the analysis of Hsp70 binding to AuNP-Ab conjugates (Figures 3 and 4), the Trf interference study by DSC reveals the presence of either AuNP-Ab conjugates alone or “fully Hsp70 loaded” AuNP-Ab conjugates, whereas AGE reveals a population of AuNP-Ab-Hsp70 complexes with different Hsp70 loads. The fluorimetric assay in the presence of Trf (Figure 5C) further confirms the interference of this plasma protein with Hsp70 binding to AuNP-Ab conjugates, as fluorescence intensity decreases as much as 27% in an Hsp70 concentration-dependent manner (Figure S4, Supporting Information). This decrease in fluorescence intensity indicates less Hsp70 binding to the AuNP-Ab conjugates loaded with fluorescent-label antigen under competitive conditions, and indicates that Trf is blocking Hsp70 binding. A comparison of the inhibitory effect of Trf on Hsp70 binding for the different techniques (as a percentage) is shown in Figure S5 of the Supporting Information. Taken together, the results of the Trf interference experiments employing three independent techniques indicate that Trf interferes with Hsp70 binding to the AuNP-Ab conjugates not by direct binding to the Ab sites, but rather indirectly, possibly by interacting with the Hsp70, blocking its Ab binding epitopes. This putative interaction of Trf with *Pf*Hsp70, a heat-shock protein that is a chaperone,^[26] finds support in the observations of Brymora et al., who found human Hsp70 to bind nonspecifically to other proteins in pull-down experiments.^[27]

2.4.2. Whole Plasma Competitive Binding

In clinical applications, AuNP-Ab based immunoassays would be used on whole blood samples. Thus, the interference of

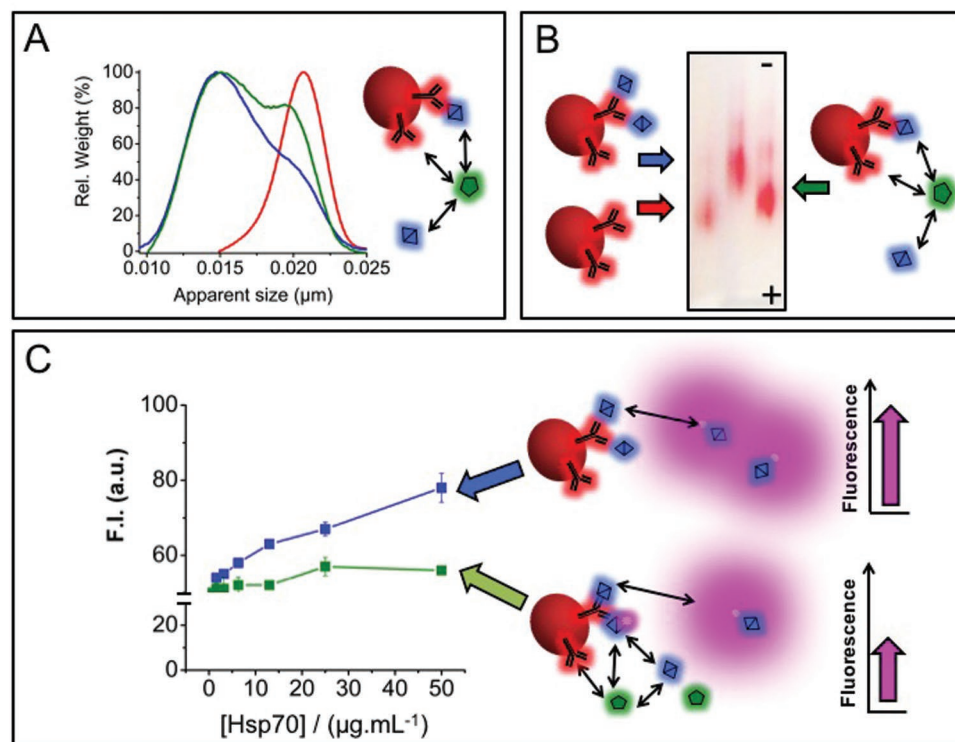


Figure 5. Transferrin (Trf) interference with Hsp70 binding to AuNP-Ab conjugates. AuNP-Ab conjugates were incubated with Hsp70 alone; or with equimolar amounts of Hsp70 and Trf. Blue diamonds represent Hsp70, and green pentagons represent Trf. A) DCS profile for AuNP-Ab conjugates alone (red profile), in the presence of Hsp70 (blue profile), and in the presence of Hsp70 and Trf (green profile). B) AGE for AuNP-Ab conjugates alone (left lane, red arrow), in the presence of Hsp70 (middle lane, blue arrow), and in the presence of Hsp70 and Trf (right lane, green arrow). C) Fluorescence intensity of the competitive immunoassay in the presence of Hsp70 only (blue trace), or in the presence of equimolar amounts of Hsp70 and Trf (green trace). Data and error bars are from three independent experiments.

whole plasma, which consists of ≈ 3700 different proteins at various concentrations, on Hsp70 binding to the AuNP-Ab conjugates was also investigated using DCS. Fluorescence spectroscopy was not employed in these experiments due to the elevated intrinsic fluorescence presented by whole plasma in control experiments (data not shown). **Figure 6** presents a comparison of the DCS relative weight size distributions for AuNP-Ab conjugates incubated with a 30 \times molar excess of Hsp70, in the presence of increasing plasma concentrations in the range of 0.1%–1.0%. Note that these plasma concentrations are significantly lower than in whole blood, and correspond to naturally occurring Trf concentrations of 4–40 $\mu\text{g mL}^{-1}$,^[25] i.e., such plasma solutions contain Trf in the concentration range utilized here to assess the influence of Trf on the binding of Hsp70 to the AuNP-Ab conjugates (Figure 5). As expected, in the absence of plasma, the shape of the DCS profile corresponds to a monomodal distribution for the AuNP-Ab conjugates alone, and to a bimodal distribution in the presence of Hsp70 (Figure 6A). Noticeably, for a plasma concentrations as low as 0.1% (Figure 6B), there is a change in the DCS profile toward the monomodal distribution, hinting at a severe impairment of Hsp70 binding in the presence of plasma proteins. This impairment of Hsp70 binding to the AuNP-Ab complexes by plasma persists at higher plasma concentrations of 0.5% (Figure 6C), and 1% (Figure 6D). No further changes were observed for higher plasma concentrations (1.5% and 3%) (data not shown).

By applying the previously described fitting model for DCS profiles, it was possible to quantify the plasma interference as inhibiting 82% of Hsp70 binding to AuNP-Ab conjugates. This inhibition by plasma can occur either by adsorbing of plasma proteins onto the Ab-AuNPs, preventing antigen recognition; or by antigen interaction and inactivation by plasma proteins. The latter would represent an amplification of the inhibitory effect proposed when only Trf was used. This observation confirms Trf as a representative protein model for the analysis of plasma interference in Hsp70-to-Ab binding in AuNP-Ab conjugates. A comparison of the inhibitory effect of Trf and plasma (at natural occurring Trf concentrations in plasma of 40 and 80 $\mu\text{g mL}^{-1}$) is shown in Figure S6 of the Supporting Information.

3. Conclusion

Complex thermodynamic and kinetic phenomena take place when antibodies bind to AuNPs to form AuNP-Ab conjugates, and when the antigen binds to these conjugates. Due to the importance of such phenomena for the rational development of AuNP-based immunoassays, alternative techniques are needed for characterizing these interactions, especially in the presence of competing interactions. Here, exploration of properties at the nanoscale such as distance-dependent fluorescence quenching; adaptation of a common biochemical technique such as

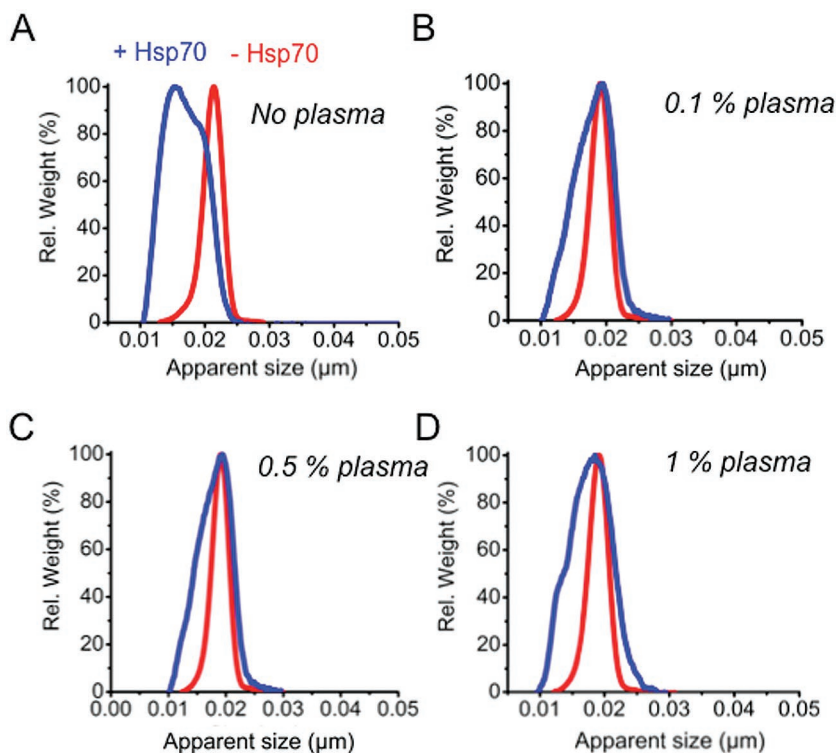


Figure 6. Whole plasma interference with Hsp70 binding by AuNP-Ab conjugates as assessed by DCS. Relative weight size distributions of AuNP-Ab conjugates alone (red lines), or AuNP-Ab incubated with Hsp70 at a molar ratio of 1:30 (blue lines), A) without plasma; or incubated with plasma at concentrations of B) 0.1%, C) 0.5%, and D) 1%.

AGE; and utilization of novel aspects of centrifugal sedimentation, were combined in an integrated analysis of the effectiveness of an immunoassay for malaria antigen (Hsp70) detection using AuNP-Ab conjugates.

When the nature of the AuNP-Ab conjugates was analyzed by DCS and AGE with increasing Ab-to-AuNP molar ratios, the formation of a single species, the AuNP-Ab complex with Ab saturation of the AuNP surface, was unequivocally identified.

DCS and AGE were also employed for the analysis of Hsp70 binding to the AuNP-Ab conjugate, revealing a different Hsp70-to-Ab binding model. In fact, two populations were detected by DCS, corresponding to either fully Hsp70-charged AuNP-Ab or to AuNP-Ab alone, whereas only one population was detected by AGE, corresponding to partially Hsp70-charged AuNP-Ab. As such, Hsp70 binding to AuNP-Ab conjugates as revealed by AGE experiments is similar to the behavior observed by both DCS and AGE for Ab binding to AuNP, in which an Ab corona grows around the AuNP as the Ab concentration is increased.

We have previously shown that a fluorescence immunoassay could determine Hsp70 binding to the AuNP-Ab conjugates in an Hsp70 concentration-dependent manner.^[15] This assay measures only the AuNP-Ab-bound Hsp70 indirectly by fluorescence quenching, and cannot distinguish between different AuNP-species. Although having less informational content, the fluorescence immunoassay is highly selective for its particular analyte. Here, we have extended the use of the fluorimetric assay to unequivocally demonstrate interference of a plasma protein (Trf) on Hsp70 binding to the AuNP-Ab conjugates. Molecular

details of the inhibition process were further revealed by DCS and AGE. In fact, while DCS pointed toward a diminished amount of the AuNP-Ab-Hsp70 complex in the presence of Trf, AGE indicated the formation of a new species with a smaller amount of Hsp70 bound than the noninhibited species. These results, and control experiments showing no interaction between Trf and AuNP-Ab conjugates, point towards Trf inhibition via a Trf-Hsp70 interaction. Whole plasma inhibition of Ab binding to the AuNP-Ab conjugate was also assessed by DCS. Again, inhibition of Hsp70 binding to AuNP-Ab conjugates was translated by this technique into diminished amounts of AuNP-Ab-Hsp70 complex, with a concomitant relative increase of free AuNP-Ab conjugates.

In conclusion, evidence is presented supporting the utilization of fluorescence spectroscopy, AGE, and DCS in the qualitative and quantitative analysis of Hsp70 binding to AuNP-Ab conjugates including under competitive binding conditions. The techniques are complementary, and each presents advantages and limitations. Importantly, AGE is a widely available and inexpensive technique, which does not require trained personnel, and is easily extendable for point-of-care applications. Here, we show for the first time that AGE can be used for the fast and inexpensive characterization of antibody-AuNP complexes regarding their specificity, sensitivity, and interference from plasma proteins. We believe that the current work will catalyze the use of AGE to elucidate complex interactions on these bio-nano-systems, in order to optimize the assay for use with clinical samples.

4. Experimental Section

Materials: AuNPs were citrate-stabilized 30 nm diameter gold colloid from British BioCell International (BBI, Cardiff, UK), and were used without further treatment. Protein determination was performed by the bicinchoninic acid method,^[28] using a kit (Sigma). UltraPure agarose for agarose gels was from Invitrogen. SDS-PAGE reagents were from BioRad. Unless otherwise stated, all other chemicals and reagents were from Sigma-Aldrich or Fluka, and were of the highest purity available.

Antibody and Antigen Sources: Production and purification of the anti-*Pf*Hsp70 monoclonal antibody 2E6 (referred to as "Ab"), and overexpression and purification of recombinant *Pf*Hsp70 protein (referred to as "Hsp70"), were as previously described.^[15] Full details of the production, purification and characterization of Ab and Hsp70, as well as for the labeling of Hsp70 with the Cy3B fluorophore, can be found in the SI under Supplementary Experimental Section.

Antibody Conjugation to Gold Nanoparticles: Equal volumes of Ab in PB (5×10^{-3} M, pH 7.2) and AuNPs solutions were mixed and incubated overnight at 4 °C to a final concentration of 0.56×10^{-9} M AuNP, with Ab to AuNP molar ratios ranging from 5 to 1000:1.

Human Plasma: Blood was withdrawn from 10 to 15 different volunteers and collected into 10 mL K₂EDTA coated tubes (BD

Bioscience). Plasma was prepared following the HUPO Plasma Proteome Project guidelines.^[29] Briefly, immediately after blood collection, each tube was inverted ten times to ensure mixing of blood with the EDTA, and subsequently centrifuged for 10 min at 1300 g at 4 °C. Equal volumes of plasma from each donor were collected into a secondary 50 mL falcon tube and then centrifuged at 2400 g for 15 min at 4 °C. Supernatant was collected (leaving ≈10% of the volume in the secondary tube) and it was then aliquoted into 1 mL cryovials and stored at -80 °C until use. The whole procedure did not take more than 3 h. When plasma was used, it was allowed to thaw at room temperature and centrifuged for 3 min at 16 200 g and used immediately. Thawed plasma was never re-frozen or re-thawed. Data presented were obtained using plasma from one donation session.

Differential Centrifugal Sedimentation: DCS measurements were performed with a CPS Disc Centrifuge (model DC24000, CPS Instruments, Florida, USA) at 22000 rpm, using an 8%–24% sucrose gradient and 0.37 μm PVP particles as internal calibration for each measurement. PBS (10 × 10⁻³ M phosphate buffer, 137 × 10⁻³ M NaCl, 2.7 × 10⁻³ M KCl, pH 7.4) was the sucrose gradient dispersant. Estimation of the protein shell thickness was performed as previously described.^[13b]

AuNP-Ab incubations with Hsp70, Trf or plasma were performed at RT for at least 2 h. AuNP-Ab conjugates were diluted from 0.58 × 10⁻⁹ M stock solutions with PB. Hsp70, Trf and plasma were diluted from stock solutions in PBS, with the final reaction mixture containing 1/3 PBS and 2/3 PB. The Hsp70 or Trf to Ab molar ratios ranged from 3 to 120, corresponding to final concentrations from 4 to 160 μg mL⁻¹ and the final plasma concentration ranged from 0.1% to 1% V/V. The final AuNP-Ab concentration was 0.056 × 10⁻⁹ M, with an Ab to AuNP molar ratio of 200:1.

Agarose Gel Electrophoresis: Gels were prepared by heating agarose in TAE buffer, 0.25×, pH 8.4, and allowing the gel to form at RT. AuNP-Ab conjugates were pelleted by centrifugation (20817 g, 4 °C, 15 min), after their pH was adjusted to 12, re-suspended in 12 μL of supernatant and mixed with 2 μL glycerol (87%) prior to loading. Agarose gels (0.5%) were run at constant voltage of 150 V (AuNP-Ab conjugates), or 300 V (AuNP-Ab-Hsp70 in the absence or presence of Trf), with a 15 cm electrode spacing, for 40 min, in TAE 0.25×, using the mini-protean system from BioRad. Digital pictures were acquired with a Canon IXUS 105 digital camera, with 12 Mega Pixels resolution, and processed with linear contrast adjustments. The electrophoretic mobility (μ) is defined as the observed rate of migration of a component (v) divided by the electric field strength (E) in a given medium.^[30] In the case of AGE, a solid support medium, only apparent values can be determined.^[30] Mobility is expressed with a negative sign, because migration of particles occurs in the opposite direction to the electrophoretic field.

AuNP-Ab incubations with Hsp70 or Trf were performed at RT for at least 2 h. AuNP-Ab conjugates were diluted from 0.58 × 10⁻⁹ M stock solutions with PB. Hsp70 and Trf were diluted from stock solutions in PBS, with the final reaction mixture containing 1/3 PBS and 2/3 PB. The Hsp70 or Trf to Ab molar ratios ranged from 0.095 to 49, corresponding to final concentrations from 0.211 to 114 μg mL⁻¹. The final AuNP-Ab concentration was 0.21 × 10⁻⁹ M, with an Ab to AuNP molar ratio of 200:1.

Fluorescence Spectroscopy: Emission spectra were recorded on a Fluorolog 3 spectrofluorimeter (Horiba Scientific, Japan) in the 500–700 nm range, where the characteristic spectrum of Cy3B is observed, with excitation at 480 nm. All samples were measured in quartz cells with 1 cm optical path length (Hellma, Germany) at RT.

AuNP-Ab incubations with Hsp70 or Trf were performed at RT for at least 2 h. Cy3B-labeled Hsp70 was added after this period, and incubated for an additional 1 h. AuNP-Ab conjugates were diluted from 0.58 × 10⁻⁹ M stock solutions with PB. Hsp70 and Trf were diluted from stock solutions in PBS, with the final reaction mixture containing 1/3 PBS and 2/3 PB. The Hsp70 or Trf to Ab molar ratios ranged from 12 to 765:1, corresponding to final concentrations from 0.78 to 50 μg mL⁻¹. The Hsp70 labelled with Cy3B (in PBS) was present at a final concentration of 17.5 μg mL⁻¹. The final AuNP-Ab concentration was 0.0047 × 10⁻⁹ M, with an Ab to AuNP molar ratio of 200:1.

UV-Vis Spectroscopy: UV-vis spectroscopy was performed in quartz cells with 1 cm path length (Hellma, Germany), using an UV-Vis spectrophotometer from UNICAM (model UV2) or Cary (model Cary 50 version 3.0 or model 6000i version 1.12). To estimate the concentration of the AuNP, the method reported by Haiss et al.^[31] was used.

Dynamic Light Scattering: Measurements were performed in a Malvern Zetasizer Nano ZS (Malvern, Worcestershire, UK) at a controlled temperature of 25 °C with light detection at 173° using the backscatter mode. Each sample was measured at least three consecutive times, with each measurement being the average of 20-submeasurements. The final AuNP-Ab concentration was 0.056 × 10⁻⁹ M, with an Ab to AuNP molar ratio of 200:1.

Peak Fit Analysis of the DCS Results: The software PeakFit (PeakFit v4.12, Seasolve Software Inc., San Jose, CA, USA) was used to fit the DCS weight distribution results in order to obtain a quantitative analysis of the populations present at each experimental condition. Two Gaussian population distributions, representing AuNP-Ab and the AuNP-Ab-Hsp70, respectively, were used as peak type chromatographic Gaussian areas. The R² for the fitted Gaussians were equal to or higher than 0.99.

Langmuir Adsorption Isotherm Fit to DCS and AGE Data: As more antibody is adsorbed at the AuNP surface, the formed conjugate increases its size, as detected by DLS (Figure 1B) and DCS (Figure 2A), and the electrophoretic mobility is reduced (AuNP-Ab conjugates become less negative), as seen by the reduced migration toward the positive electrode (Figure 2B). Eventually the mobility reaches a plateau (Figure 2A,B) corresponding to saturation of the AuNP surface with Ab. This approach led to a Langmuir adsorption isotherm type (Equation (1))

$$\frac{A}{A_{\max}} = \frac{K_L \times [L]}{1 + K_L \times [L]} \quad (1)$$

in which A/A_{max} is a measure of the fraction of adsorbed antibodies per AuNP as accessed by DCS (Figure 2B), the % of AuNP-Ab-Hsp70 conjugates (Figure 4B), or the electrophoretic mobility variation Δ μ, (Figure 2D), L is Ab (Figure 2B,D), or Hsp70 (Figure 4B), and K_L is the binding constant in M⁻¹. In order to fit an isotherm to the experimental values from Figures 2 and 4, that is standardized for the AuNP concentration, we used Origin 6.1, and Equation (2)

$$A = \frac{A_{\max} \times K'_L \times R}{1 + K'_L \times R} \quad (2)$$

in which R is the Ab to AuNP molar ratio, or the Hsp70 to AuNP molar ratio, and K'_L is the binding constant corresponding to the value of the inverse of the concentration ratio, 1/R, for one-half A_{max}.

Supporting Information

Supporting Information is available from the Wiley Online Library or from the author.

Acknowledgements

The authors thank Isabel Silva (UCIBIO, REQUIMTE, Portugal) for help in the purification of the 2E6 antibody and PfHsp70 antigen, and Patrícia Meireles (Prudência Lab, IMM, Portugal) for immunofluorescence microscopy analysis of the purified 2E6 antibody. This work was supported by the European Science Foundation Research Networking Program, "EpitopeMap" (exchange visit to UCD by M.C. and short visit by R.F.) and the Luso-American Foundation, Portugal (Grant FLAD-LACR, to R.F. and M.P.). Further support came from the Unidade de Ciências Biomoleculares Aplicadas-UCIBIO which was financed by

Portuguese national funds from FCT/MEC (UID/Multi/04378/2013) and co-financed by the ERDF under the PT2020 Partnership Agreement (POCI-01-0145-FEDER-007728), to M.C., E.P., and R.F.; and from a SFI Industry fellowship 15/IFA/3057 awarded to M.M. Part of this work was conducted under the framework of the INSPIRE programme, funded by the Irish Government's Programme for Research in Third Level Institutions, Cycle 4, National Development Plan 2007–2013 (M.M.).

Received: July 14, 2016

Revised: August 23, 2016

Published online: October 25, 2016

- [1] a) A. V. Page, W. C. Liles, *Virulence* **2013**, *4*, 507; b) M. Rubio, Q. Bassat, X. Estivill, A. Mayor, *Malaria J.* **2016**, *15*, 167.
- [2] W.H.O., Geneva, Switzerland, **2015**.
- [3] N. L. Anderson, N. G. Anderson, *Mol. Cell. Proteomics* **2002**, *1*, 845.
- [4] a) C. Longo, A. Patanarut, T. George, B. Bishop, W. Zhou, C. Fredolini, M. M. Ross, V. Espina, G. Pellacani, E. F. Petricoin, L. A. Liotta, A. Luchini, *PLoS ONE* **2009**, *4*, e4763; b) A. Luchini, C. Longo, V. Espina, E. F. Petricoin III, L. A. Liotta, *J. Mater. Chem.* **2009**, *19*, 5071; c) D. Tamburro, C. Fredolini, V. Espina, T. A. Douglas, A. Ranganathan, L. Ilag, W. Zhou, P. Russo, B. H. Espina, G. Muto, E. F. Petricoin 3rd, L. A. Liotta, A. Luchini, *J. Am. Chem. Soc.* **2011**, *133*, 19178.
- [5] M. Peixoto de Almeida, E. Pereira, P. Baptista, I. Gomes, S. Figueiredo, L. Soares, R. Franco, in *Comprehensive Analytical Chemistry*, Amsterdam, Vol. 66 (Eds: V. Miguel, I. L.-L. Ángela), Elsevier, **2014**, p. 529.
- [6] a) M. A. Nash, J. N. Waitumbi, A. S. Hoffman, P. Yager, P. S. Stayton, *ACS Nano* **2012**, *6*, 6776; b) D. Y. Pereira, R. Y. T. Chiu, S. C. L. Zhang, B. M. Wu, D. T. Kamei, *Anal. Chim. Acta* **2015**, *882*, 83.
- [7] a) D. Quesada-González, A. Merkoçi, *Biosens. Bioelectron.* **2015**, *73*, 47; b) R. Wilson, *Chem. Soc. Rev.* **2008**, *37*, 2028.
- [8] X. Liu, Q. Dai, L. Austin, J. Coutts, G. Knowles, J. Zou, H. Chen, Q. Huo, *J. Am. Chem. Soc.* **2008**, *130*, 2780.
- [9] S. van der Heide, D. A. Russell, *J. Colloid Interface Sci.* **2016**, *471*, 127.
- [10] C. Parolo, A. de la Escosura-Muñiz, E. Polo, V. Grazú, J. M. de la Fuente, A. Merkoçi, *ACS Appl. Mater. Interfaces* **2013**, *5*, 10753.
- [11] a) A. Akesson, M. Cardenas, G. Elia, M. P. Monopoli, K. A. Dawson, *RSC Adv.* **2012**, *2*, 11245; b) T. Cedervall, I. Lynch, S. Lindman, T. Berggard, E. Thulin, H. Nilsson, K. A. Dawson, S. Linse, *Proc. Natl. Acad. Sci. USA* **2007**, *104*, 2050; c) M. Mahmoudi, I. Lynch, M. R. Ejtehadi, M. P. Monopoli, F. B. Bombelli, S. Laurent, *Chem. Rev.* **2011**, *111*, 5610; d) M. P. Monopoli, D. Walczyk, A. Campbell, G. Elia, I. Lynch, F. B. Bombelli, K. A. Dawson, *J. Am. Chem. Soc.* **2011**, *133*, 2525; e) A. E. Nel, L. Madler, D. Velegol, T. Xia, E. M. Hoek, P. Somasundaran, F. Klaessig, V. Castranova, M. Thompson, *Nat. Mater.* **2009**, *8*, 543.
- [12] J. Sund, H. Alenius, M. Vippola, K. Savolainen, A. Puustinen, *ACS Nano* **2011**, *5*, 4300.
- [13] a) E. Casals, T. Pfaller, A. Duschl, G. J. Oostingh, V. Puentes, *ACS Nano* **2010**, *4*, 3623; b) D. Walczyk, F. B. Bombelli, M. P. Monopoli, I. Lynch, K. A. Dawson, *J. Am. Chem. Soc.* **2010**, *132*, 5761.
- [14] a) D. Maiolo, P. Bergese, E. Mahon, K. A. Dawson, M. P. Monopoli, *Anal. Chem.* **2014**, *86*, 12055; b) S. Milani, F. B. Bombelli, A. S. Pitek, K. A. Dawson, J. Radler, *ACS Nano* **2012**, *6*, 2532; c) S. Wan, P. M. Kelly, E. Mahon, H. Stöckmann, P. M. Rudd, F. Caruso, K. A. Dawson, Y. Yan, M. P. Monopoli, *ACS Nano* **2015**, *9*, 2157.
- [15] B. Guirgis, C. Sá e Cunha, I. Gomes, M. Cavadas, I. Silva, G. Doria, G. Blatch, P. Baptista, E. Pereira, H. Azzazy, M. Mota, M. Prudêncio, R. Franco, *Anal. Bioanal. Chem.* **2012**, *402*, 1019.
- [16] H. A. Krebs, *Annu. Rev. Biochem.* **1950**, *19*, 409.
- [17] a) W. J. Parak, T. Pellegrino, C. M. Micheel, D. Gerion, S. C. Williams, A. P. Alivisatos, *Nano Lett.* **2002**, *3*, 33; b) D. Zanchet, C. M. Micheel, W. J. Parak, D. Gerion, A. P. Alivisatos, *Nano Lett.* **2000**, *1*, 32.
- [18] a) D. Bartczak, A. G. Kanaras, *Langmuir* **2011**, *27*, 10119; b) U. Pyell, *Electrophoresis* **2010**, *31*, 814.
- [19] a) J. Foote, H. N. Eisen, *Proc. Natl. Acad. Sci. USA* **1995**, *92*, 1254; b) H. Fukunishi, J. Shimada, K. Shiraishi, *Biochemistry* **2012**, *51*, 2597.
- [20] H. G. Lee, *J. Chromatogr. A* **1997**, *790*, 215.
- [21] E. Gasteiger, C. Hoogland, A. Gattiker, S. e. Duvaud, M. R. Wilkins, R. D. Appel, A. Bairoch, in *The Proteomics Protocols Handbook* (Ed: J. M. Walker), Humana Press, Totowa, NJ **2005**, p. 571.
- [22] E. Betgovargez, V. Knudson, M. H. Simonian, *J. Biomol. Tech.: JBT* **2005**, *16*, 306.
- [23] E. Boisselier, D. Astruc, *Chem. Soc. Rev.* **2009**, *38*, 1759.
- [24] A. Salvati, A. S. Pitek, M. P. Monopoli, K. Prapainop, F. B. Bombelli, D. R. Hristov, P. M. Kelly, C. Aberg, E. Mahon, K. A. Dawson, *Nat. Nano* **2013**, *8*, 137.
- [25] *The Plasma Proteins: Structure, Functions, and Genetic Control*, Vol. 4, Academic, Orlando, FL **1984**.
- [26] G. Banumathy, V. Singh, U. Tatu, *J. Biol. Chem.* **2002**, *277*, 3902.
- [27] A. Brymora, V. A. Valova, P. J. Robinson, *Current Protocols in Cell Biology* (Eds: Juan S. Bonifacino, Joe B. Harford, Jennifer Lippincott-Schwartz, Kenneth M. Yamada), **2004**, New York, John Wiley & Sons, Chap. 17, Unit 17.15.
- [28] P. K. Smith, R. I. Krohn, G. T. Hermanson, A. K. Mallia, F. H. Gartner, M. D. Provenzano, E. K. Fujimoto, N. M. Goeke, B. J. Olson, D. C. Klenk, *Anal. Biochem.* **1985**, *150*, 76.
- [29] A. J. Rai, C. A. Gelfand, B. C. Haywood, D. J. Warunek, J. Yi, M. D. Schuchard, R. J. Mehig, S. L. Cockrill, G. B. I. Scott, H. Tammen, P. Schulz-Knappe, D. W. Speicher, F. Vitzthum, B. B. Haab, G. Siest, D. W. Chan, *Proteomics* **2005**, *5*, 3262.
- [30] G. Ferard, *Pure Appl. Chem.* **1994**, *66*, 891.
- [31] W. Haiss, N. T. K. Thanh, J. Aveyard, D. G. Fernig, *Anal. Chem.* **2007**, *79*, 4215.